AGU
ADVANCING EARTH AND SPACE SCIENCES

Earth and Space Science

Key Points:

- We present the first 3D resistivity model of Portugal mainland using data from 31 broadband Magnetotelluric stations spaced in 50 × 50 grid
- Description of the large-scale resistive/conductive crustal domains characterized by a less heterogeneous central and northern regions
- Interconnected graphite in structural discontinuities, possibly forming a regional mid-crustal decollement

Supporting Information:

Supporting Information may be found in the online version of this article.

Correspondence to:

P. Baltazar-Soares,
pabsoares@fc.ul.pt

Author Contributions:

Conceptualization: P. Baltazar-Soares
Data curation: P. Baltazar-Soares, F. J. Martínez-Moreno, J. Pous
Formal analysis: P. Baltazar-Soares, J. Alves Ribeiro, F. A. Monteiro Santos, P. Ribeiro, M. A. Pais, A. Mateus, J. Pous
Funding acquisition: M. A. Pais
Investigation: P. Baltazar-Soares, F. J. Martínez-Moreno, J. Alves Ribeiro

Crustal Imaging of Portugal Mainland Using Magnetotelluric Data

P. Baltazar-Soares[1] , F. J. Martínez-Moreno[2] , J. Alves Ribeiro[3] , F. A. Monteiro Santos[1], P. Ribeiro[4] , M. A. Pais[3] , A. Mateus[1], and J. Pous[5]

[1]Universidade de Lisboa, Faculdade de Ciências, Instituto Dom Luiz, Lisboa, Portugal, [2]Departamento de Geodinámica, Estratigrafía y Paleontología, Universidad Complutense de Madrid, Madrid, Spain, [3]Department of Physics, CITEUC, University of Coimbra, Coimbra, Portugal, [4]Geophysical and Astronomical Observatory, CITEUC, University of Coimbra, Coimbra, Portugal, [5]Departament de Dinàmica de la Terra i de l'Oceà, Universitat de Barcelona, Barcelona, Spain

Abstract The comprehensive mapping of resistivities in depth and its interpretation is of great importance to unravel the electrical properties of deep-seated rocks, providing significant insights into the structure of the crust. The first 3D resistivity model for Portugal mainland is here reported using data from 31 broadband MT soundings spaced 50 × 50 km apart. The model shows large crustal volumes with contrasting resistivity values. The central and northern regions are characterized by a high resistivity crustal domain spreading in-depth (10^3–10^5 Ω.m) that correlates well with voluminous granitoid bodies and high-grade metamorphic rocks. To the west and the south, roughly corresponding to the Portuguese Western Shore and the South Portuguese Zone (SPZ) respectively, the crustal resistivity tends to decrease unevenly to values between 1 and 10^3 Ω.m. Interconnected graphite in structural discontinuities, possibly forming a regional mid-crustal *décollemen*t at ≈13–15 km depth, are highlighted by multiple low resistivity crustal domains (1–100 Ω.m). Similarly, the model reveals a very large E-W low resistivity crustal domain in SPZ possibly representing a deep-seated major *décollement*. The present study aims to contribute to a better understanding of the physical properties characterizing the concealed crust in Portugal mainland, providing also indirect information on its composition and structure.

Plain Language Summary Portugal is located in the western part of Europe and most of its geological background is part of the Iberian Massif, an ancient block of continental lithosphere composed of several geotectonic units that differ in rock composition and structure. The geological characteristics of these main units, as well as the structures that separate them, potentially generate distinctive geoelectric signatures. Over the years, most electromagnetic surveys have been carried out on a regional scale. The focus has always been on the specific features of certain zones of the Portugal mainland, so it has not been possible to obtain a complete picture of the large-scale structures that extend over the entire crust, especially in the northern part of the country. Therefore, the 3D resistivity model obtained through an electromagnetic method called Magnetotelluric (MT), allows us to have a complete image of the crust up to ≈40 km deep. The results contribute to a better characterization of the crust and reveal that the crustal segment extending beneath the central and northern regions of the Portuguese mainland is much less heterogeneous than its southern counterpart, providing important information to issues addressed in various fields of geosciences (e.g., Space Weather, Mineral, and Hydrocarbon exploration).

1. Introduction

Portugal is located in the western part of Europe and most of its geological background is part of the Iberian Massif, the westernmost European segment of the Late Paleozoic Variscan orogenic belt (Figure 1a). The Iberian Massif is composed of several geotectonic units with contrasting differences in rock composition and structure (e.g., Azor et al., 2019; Simancas, 2019; and references therein). In the Portuguese segment of the Iberian Massif, the represented geotectonic units are, from north to south: the Galicia Trás-os-Montes Zone (GTMZ), Central-Iberian Zone (CIZ), Ossa-Morena Zone (OMZ) and South Portuguese Zone (SPZ). The geological attributes of these main units, as well as of the first order structures that separate them, potentially generate distinctive geoelectrical signatures. The study area has been the subject of several electromagnetic surveys (Almeida et al., 2001, 2005; Alves Ribeiro et al., 2017; Farzamian et al., 2018; Monteiro Santos et al., 1995, 1999; Monteiro Santos, Mateus, et al., 2002; Monteiro Santos, Matos, et al., 2002; Muñoz et al., 2005, 2008; Pous et al., 2004;

Methodology: P. Baltazar-Soares, F. J. Martínez-Moreno, J. Alves Ribeiro, F. A. Monteiro Santos, M. A. Pais, A. Mateus
Project Administration: M. A. Pais
Software: P. Baltazar-Soares, J. Alves Ribeiro
Supervision: F. A. Monteiro Santos, M. A. Pais
Validation: P. Baltazar-Soares, F. J. Martínez-Moreno, J. Alves Ribeiro, F. A. Monteiro Santos, P. Ribeiro, M. A. Pais, A. Mateus, J. Pous
Visualization: P. Baltazar-Soares, F. J. Martínez-Moreno, J. Alves Ribeiro, F. A. Monteiro Santos, P. Ribeiro, M. A. Pais, A. Mateus, J. Pous
Writing – original draft: P. Baltazar-Soares, A. Mateus
Writing – review & editing: P. Baltazar-Soares, F. J. Martínez-Moreno, J. Alves Ribeiro, F. A. Monteiro Santos, P. Ribeiro, M. A. Pais, A. Mateus

Vieira da Silva et al., 2007) and seismic surveys (Arroucau et al., 2021; Dündar et al., 2016; Prodehl et al., 1975; Simancas et al., 2001, 2003; Veludo et al., 2017). As a result of these surveys, discontinuous conductive strips in the mid-crust were recognized, especially across the OMZ and SPZ, along with a possible regional crustal detachment at depths of ~15 km. Although most of the electromagnetic research has been developed on a regional scale, the main focus was always specific features displayed by particular zones of Portugal mainland, therefore not allowing a complete image of large-scale structures extending across the whole crust, especially to the northern part of the country.

The knowledge of sub-surface physical properties, such as resistivity/conductivity, is essential for better characterization and understanding of the crustal structure/composition and can provide important information to issues addressed in various fields of geosciences, namely in mineral and hydrocarbon exploration surveys (Corseri et al., 2017; Graham et al., 2021). Moreover, in recent years, information on the electrical properties of crust and mantle has also been used to estimate the effect of Space Weather events on long and grounded conducting infrastructures, such as power lines (e.g., Alves Ribeiro et al., 2021). The Magnetotelluric (MT) method uses natural electromagnetic fields to estimate the spatial arrangement of electrical conductivity in depth. This method has been widely used to characterize and study the lithosphere architecture in regions with a complex geological background (e.g., Bai et al., 2010; González-Castillo et al., 2015; Wannamaker, 2002; Zhao et al., 2012). In this work, we present the first 3D resistivity model of Portugal mainland obtained by inversion of MT data to characterize the whole crustal structure below the country's surface.

2. Geologic Setting

A comprehensive and up-to-date review of the geological characteristics displayed by the Iberian Massif and the resulting implications for the reconstruction of its geodynamic evolution during the Variscan cycle can be found in a recently published collection of articles forming the second volume of a series of five addressing the Geology of Iberia (https://link.springer.com/book/10.1007/978-3-030-10519-8). Considering the purpose of the present study, the most relevant features of the Iberian Massif can be summarized as follows:

1. The Iberian Massif represents an old block of continental lithosphere formed as a result of a long-lasting geodynamic evolution, culminating with the development of an orogenic belt during the Late Paleozoic. The orogenic belt build-up involved the convergence and left-lateral oblique collision of the Laurasia and Gondwana continents during the Variscan Cycle by the consumption/subduction of the Rheic Ocean (e.g., Simancas, 2019 and references therein).

2. Several, well-established, geotectonic units compose the Iberian Massif (e.g., Dias & Ribeiro, 1995; Julivert et al., 1972, 1974; Lotze, 1945; Martínez-Catalán et al., 2009, 2014; Ribeiro et al., 1979, 2007). In Portugal mainland (Figure 1), from north to south, these are the GTMZ, CIZ, and the OMZ, all showing a Gondwanan affinity, and the SPZ displaying a Laurasian affinity. These geotectonic units are bounded by first order structures, often preserving evidence of multiple reactivation events. The Main Trás-os-Montes Thrust (MTMt) separates the GTMZ from CIZ. The Tomar-Portalegre-Badajoz-Córdoba shear zone (TPBCsz) represents the most conspicuous structural separation of CIZ from OMZ. The Porto-Tomar-Ferreira do Alentejo shear zone (PTFAsz) defines the westernmost limit of CIZ putting it in contact with Mesozoic sequences of the Lusitanian Basin or with high-grade metamorphic units ascribed to the OMZ in conventional tectonostratigraphic correlations or to the Finisterra Terrane in recent proposals of geodynamic reconstructions (Moreira et al., 2019, and references therein). The Ferreira-Ficalho thrust zone (FFtz) marks the present contact between OMZ and two exotic terranes, indicating the Variscan suture, to the south: the Pulo do Lobo Terrane, usually interpreted as an accretionary prism, and the tectonically dismembered Beja-Acebuches Ophiolite Complex (Quesada et al., 1994, 2019; Ribeiro et al., 2010, and references therein). The FFtz is displaced by the ENE-WSW, sub-vertical Aroche-Ficalho strike-slip fault and, according to the available data (Figueiras et al., 2002; Mateus et al., 1999), it should represent a shallow expression of a re-activated deep and more complex structure developed in the course of the OMZ-SPZ late-collision stages (see also Vieira da Silva et al., 2007). The present-day northern limit of the Algarve Basin is dominated by E-W to ENE-WSW trending fault zones (a structural inheritance from the Variscan orogeny—Terrinha, 1998), affecting the unconformity between the Carboniferous basement and the Triassic (-Lower Jurassic) basin sediments (Ramos et al., 2016, and references therein)
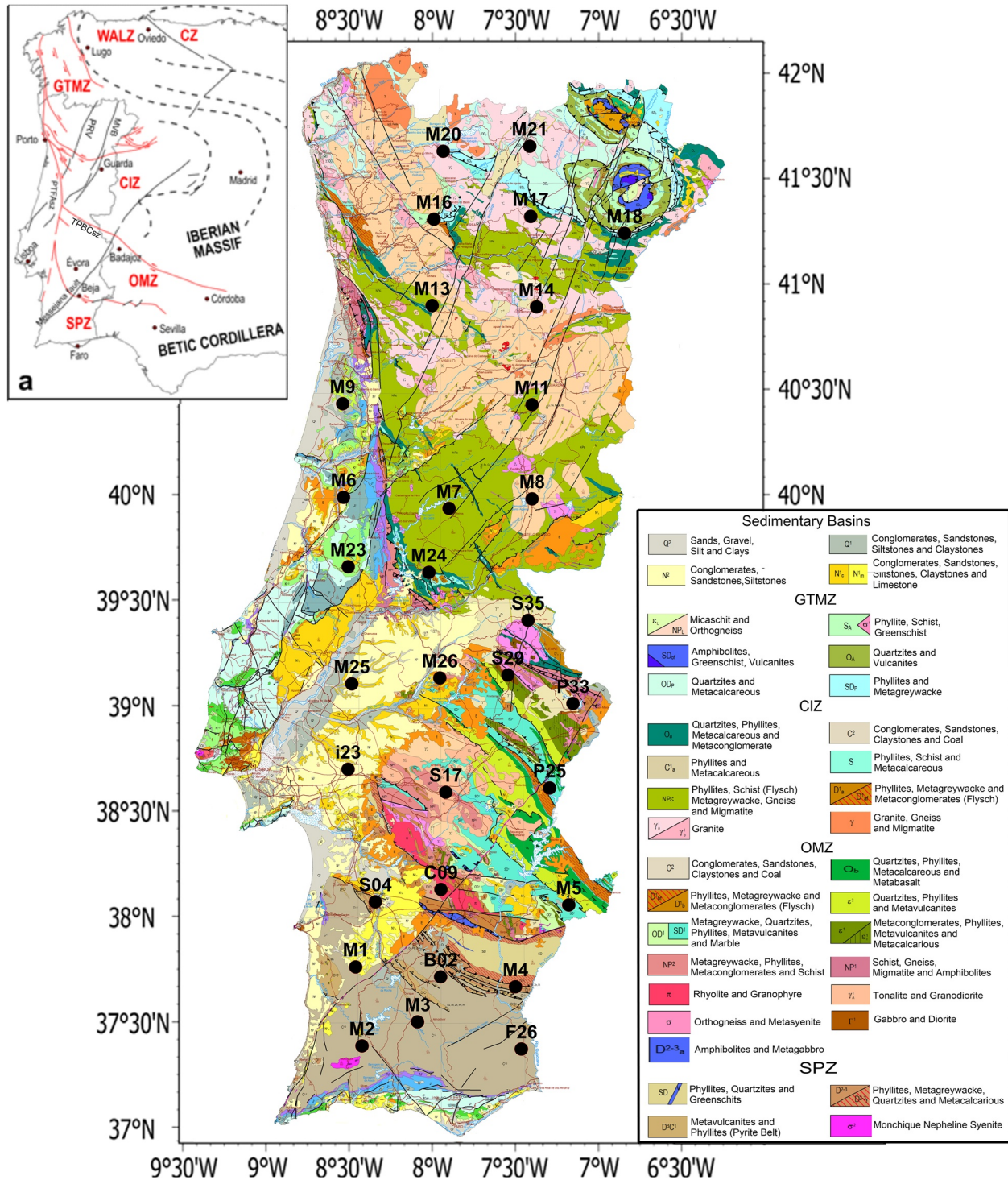
Figure 1. Geological map of Portugal mainland. (a) Geotectonic units of the Iberian Massif; (b) Lithological units; black points correspond to the MT stations. The solid black lines represent fault zones. The tectonostratigraphic units are represented by the red dashed lines. CZ, Cantabrian Zone; WALZ, West Asturian-Leonese Zone; GTMZ, Galicia Trás-os-Montes Zone; CIZ, Central Iberian Zone; OMZ, Ossa Morena Zone; SPZ, South Portuguese Zone. Source: Laboratório Nacional de Energia e Geologia (LNEG), geological map scale 1:1000000. *Note*. MT station F26 is identified as F16 or F10 in Figures 3 and 5.

3. The uniqueness of GTMZ is provided by the Bragança and Morais allochthonous massifs, stacked above the (widely siliciclastic) Parautochthonous Thrust Complex overthrusting the CIZ autochthon (e.g., Da Silva et al., 2015; Martínez Catalán et al., 2019; Ribeiro, 1974, 1981). The tectonic pile forming these allochthonous massifs comprises, from bottom to top: (a) a basal thrust complex, involving mostly siliciclastic and volcanic

units, known as the Lower Allochthonous Thrust Complex; (b) an intermediate exotic terrane of oceanic nature, branded Northern Ophiolite Terrane; and (c) a complex high-grade metamorphic terrane, labeled Upper Allochthonous (Mateus et al., 2016 and references therein). The Bragança and Morais massifs are part of an ensemble of mega-klippen extending from Galicia (Spain) to Trás-os-Montes (NE Portugal) that include the Cabo Ortegal and Órdenes massifs and the Malpica-Tuy Belt.

4. Present-day exposures of the CIZ autochthon are composed of several, siliciclastic-dominated, litho-stratigraphic successions from Neoproterozoic to Paleozoic in age, preserving effects of multiphase deformation and of metamorphic recrystallization, most of the times under greenschist facies conditions but reaching higher grades when contiguous or included in thermal domes (e.g., Azor et al., 2019; Gutiérrez-Marco et al., 2019; Oliveira, González-Clavijo, et al., 2019; Ribeiro, Reche, et al., 2019; Sánchez-García et al., 2019). Some of these litho-stratigraphic successions also comprise calc-silicate rocks and/or different types of volcanic/volcaniclastic rocks, which may locally develop accumulations of considerable thickness. To the south, namely in the OMZ, the Neoproterozoic to Paleozoic litho-stratigraphic successions are more diverse in facies, being noteworthy the much higher abundance of carbonate (including dolostones) and volcanic rocks (regularly forming bimodal sequences) in common sections of the Lower Cambrian and the Upper Cambrian to Ordovician (e.g., Azor et al., 2019; Gutiérrez-Marco et al., 2019; Oliveira, González-Clavijo, et al., 2019; Ribeiro, Reche, et al., 2019; Sánchez-García et al., 2019). The OMZ litho-stratigraphic successions also display effects of multiphase deformation and metamorphism, which usually grades from greenschist to transitional greenschist-amphibolite facies conditions. Note, however, that higher metamorphic grades and/or complex evolving paths typify the rock units observed across the OMZ northern and southern borders, forming the Blastomylonitic Belt and the Southern Crystalline Belt, respectively. In SPZ (Oliveira, Quesada, et al., 2019), the exposed litho-stratigraphic successions are confined to the Paleozoic and form two main pre-orogenic mega-sequences (the Givetian to Fammenian Phyllite-Quartzite Group and the Late Fammenian to Late Visean Volcano-Sedimentary Complex) followed by a syn-orogenic flysch sequence (the Upper Visean to Sepkhuvian-Moscovian Baixo Alentejo Flysch Group). The multiphase deformation accommodated by these three sequences generated a thin-skinned fold/thrust belt along with metamorphic recrystallization under increasingly lower PT conditions from NE (greenschist facies) to SW (prehnite-pumpellyite).

5. The Neoproterozoic to Paleozoic litho-stratigraphic successions observed in GTMZ, CIZ, OMZ, and SPZ are intruded by different igneous rocks forming various granitoid suites at places complemented with noteworthy arrays of gabbros/diorites (Ribeiro, Castro, et al., 2019). Syn-to late-orogenic granitoid batholiths, generated and emplaced in the Late Paleozoic, are the most voluminous, spreading all over the Iberian Massif but with particular prominence in CIZ. The most significant gabbro/diorite array (the Beja Igneous Complex) was also emplaced during the Carboniferous and extends along ~100 km of the OMZ southwestern border. Older granitoid plutons, documenting an important magmatic event at the Cambrian-Ordovician boundary (Sánchez-García et al., 2019), are also present in CIZ and may develop bodies of significant volume, quite often being surrounded by (early) syn-orogenic granites. Granitoid rocks ascribed to the Cadomian cycle are minor and essentially confined to the OMZ-CIZ transitional domains.

6. Late strike-slip fault zones developed in the waning stages of the Variscan orogeny, intersect all the previous structures and rock units, sometimes reactivating segments of pre-existent syn-orogenic regional shear zones (e.g., Arthaud & Matte, 1975; Marques et al., 2002). The three most remarkable elements of this Late-Variscan fracture network are indicated in Figure 1: the Manteigas-Vilariça-Bragança fault zone (MVB), the Penacova-Régua-Verín fault zone (PRV), and the Messejana fault zone. The mechanical role of the Late-Variscan fracture network during the Alpine cycle is also worthy of mention because of the influence played in the tectonic segmentation documented for the marginal Mesozoic basins, thus indirectly ruling the progression of many sedimentary processes in both the Lusitanian Basin and the Algarve Basin, respectively to the W and S of the Iberian Massif. During the rifting phases, some of these fault zones were successively reactivated and also acted as preferred conduits for basaltic magma rising, as clearly proved for the Messejana fault zone considering the multiple injections of dolerite rocks (Cebriá et al., 2003; Martins, 1991; Silva et al., 2008) and distinct displacements caused in geological formations of different ages. Later on, during the tectonic inversion experienced by these basins from the Late Cretaceous to early Miocene, the recurrent reactivation of many of these fault zones (along with other regional shear zones) generated a significant relief rejuvenation of the Iberian Massif. This led to evident Variscan basement uplifts (namely in the central domain of CIZ) and to the development of intra-mountain or peripheral Cenozoic basins, such as the Ponsul or the Tagus-Sado basins.

3. Magnetotelluric Data

The MT method measures simultaneously the natural magnetic and electric fields in orthogonal directions through the time variations of the magnetic field. The oscillating magnetic fields induce oscillating electric fields in the conducting earth, and both can be measured at the earth's surface (Cagniard, 1953; Tikhonov, 1950; Vozoff, 1991). The measured horizontal components of the electric ($\vec{E}$) and magnetic ($\vec{H}$) fields are related in the frequency domain by a frequency dependent, complex 2×2 impedance tensor ($\overline{Z}$) (Berdichevsky, 1960) as $\vec{E} = \overline{Z}\vec{H}$, where:

$$\begin{pmatrix} E_x \\ E_y \end{pmatrix} = \begin{pmatrix} Z_{xx} & Z_{xy} \\ Z_{yx} & Z_{yy} \end{pmatrix} \begin{pmatrix} H_x \\ H_y \end{pmatrix} \tag{1}$$

The apparent resistivity ($\rho_{a\,ij}$) and phase (φ_{ij}) are estimated from the complex Z tensor elements and used to estimate the subsurface resistivity,

$$\rho_{a\,ij} = \frac{1}{\mu_0 \omega}|Z_{ij}|^2$$
$$\varphi_{ij} = \tan^{-1}\left(\frac{Im\{Z_{ij}\}}{Re\{Z_{ij}\}}\right) \tag{2}$$

where μ_0 is the free-space magnetic permeability, ω is the angular frequency and Z_{ij} ($i, j = x, y$) the components of the impedance tensor. The data used were obtained by compiling results of 31 MT soundings (Figure 1b, black dots) acquired with an approximate site spacing of a 50×50 km grid. Ten MT soundings were carried out in the southern part of Portugal between 1997 and 2002 using ADU03E and ADU06 data loggers, both from Metronix (Almeida et al., 2001, 2005; Alves Ribeiro, 2018; Pous et al., 2004; Vieira da Silva et al., 2007). The most recent MT soundings (21) were conducted in different areas of Portugal mainland during the 2018–2020 period and using the ADU07 equipment. All stations were acquired within 48 hr.

The electric field components (E_x, E_y) were acquired in the N-S and E-W directions with a dipole length of about 100 m. Frequencies sampled ranged from 0.001 Hz to 10 kHz using single station recordings of both orthogonal horizontal components of the electric and magnetic fields (H_x, H_y). Due to landscape conditions, the vertical magnetic component (H_z) could not be retrieved in most soundings, therefore hindering the use of tipper information in the 3D inversion.

The magnetotelluric time series were processed using the MAPROS, a processing software developed by Metronix, which is based on the robust processing technique reported in Egbert and Booker (1986). Different signal processing steps were implemented: the dimensionless coherence parameter, computed from the correlation between the measured electric field and the electric field estimated from the estimated impedance and measured magnetic field, expresses the level of random noise in MT measurements. Only data with coherence above 0.6 were considered for this study; the data were collected from three frequency bands at the following sampling rates: 8,192, 512, and 128 Hz. The long-period time series were obtained from the decimation of the 128 Hz band, which involves sub-sampling and low-pass filtering of the data; the MT impedance tensor is evaluated at certain frequency values, obtained by merging different frequencies represented in the data through the use of a Parzen window. Different Fast Fourier Transform (FFT) lengths were used with a variable Parzen radius that depends on the variation of the FFT for different frequencies and is gradually adjusted.

4. 3D Inversion

For the 3D inversion of the MT data, we used the Modular Electromagnetic Inversion System (ModEM), which is based on a finite-difference algorithm that uses the nonlinear conjugate gradient method for optimization (Egbert & Kelbert, 2012; Kelbert et al., 2014).

The model grid consists of $45 \times 35 \times 58$ cells in horizontal and vertical directions. The inner part comprises a uniform mesh of $25 \times 15 \times 58$ cells with 25 km width in the X and Y directions (Miensopust, 2017). The central part is padded with 10 and 11 planes where cell sizes increase laterally by a factor of 1.3, in the X and Y direc-

tions, respectively (Figure S2 in Supporting Information S1). The vertical thickness is 25 m for the first layer; the subsequent layer thickness increases successively by a factor of 1.2. A coarse 3D bathymetry of the Atlantic and Mediterranean (Amante & Eakins, 2009) with a fixed seawater resistivity of 0.3 Ω.m was included as a priori information.

Several inversions were performed considering different initial resistivity models, based on the previous model (Monteiro et al., 2003) (Figure S1 and Table S1 in Supporting Information S1). Due to the poor quality of some impedance diagonals (Figure S3 in Supporting Information S1), only the off-diagonal components of the impedance tensor (Z_{xy}, Z_{yx}) were included with a 5% margin of error. Using the full impedance would increase the total nRMS by 55%. The ModEM program has been effective in minimizing the effects of static shifts (Meqbel et al., 2014; Tietze and Ritter, 2013). This is achieved by introducing a scattered conductivity distribution in the near-surface layers to accurately model the data. The exit criteria for the inversion were nRMS <1.05 or $\lambda < 10^{-8}$ during the model updating. The final model, which had a better data fit between the observed and calculated data and a lower nRMS of 1.96, was reached after 148 iterations (Figure 2 and Figure S4 and Table S1 in Supporting Information S1).

4.1. Sensitivity Analyses

The analysis of the depth of investigation was performed using an empirical procedure. The 3D final model was kept to a certain (variable) depth and below that depth, it was replaced by the values of the initial model. In this way, we can test how far in depth the model is constrained by the data. In performing the sensitivity analysis, several forward models were created for different depth constraints (10, 20, 30, 40, and 50 km). The impact on the data is shown by comparing the nRMS of each forward model with the nRMS of the final model (Figures S5 and S6 in Supporting Information S1). The closer the two RMS values are, the less sensitive the data is to changes, that is, the limit by which the data must be interpreted. In order to infer the robustness of the main structures we performed two inversions with different initial models at the crust level (Model A = 10 Ω.m; Model B = 1,000 Ω.m) (Figure S7 in Supporting Information S1). The sensitivity analyses led to a depth of investigation of ~40 km.

4.2. Anomalies Analyses

The conductive anomalies identified in our model (Figures 4 and 5) are mostly linked to individual stations. In order to demystify their significance for the model and relatively nearby stations, we performed several forward models (Figure 3), in which the values of the anomalies (C1, C2, C3, C4, and C5) were replaced by different values of resistivity (10, 50, 100, 500, 1,000, 5,000, and 10,000 Ω.m). All % values are related to the nRMS value of the best fit model.

The results in general show that above a certain resistivity value, the nRMs value increases significantly for most anomalies.

In the case of C1, the nRms values of stations M11 and M9 are affected by variations in the resistivity values >100 Ω.m, with a percentage variation of nRMS of 65% and 13% respectively.

Regarding the C2 anomaly, the nRMS values remain low for resistivity values below 100 Ω.m, with a later significant increase that is more pronounced at station S29, with effects on the total nRMS. Note that for resistivity values below 50 Ω.m, the nRms value is 0.2% lower than the best model nRMS.

For the C3 anomaly, the behavior of the nRMS values differs between the two stations. There is a pronounced increase in nRMS for resistivity values >50 Ω.m in station S17, with a percentage variation with respect to the best model nRMS of 150%. At station i23, the most significant increase is observed for resistivity values >100 Ω.m, with a variation percentage of 51%. There is a gradual increase in the total nRMS with increasing C3 resistivity.

As for the C4 anomaly, the forward model was only performed for station M5, which is relatively far from the other stations. The nRMS value remains low for resistivities <50 Ω.m, with a subsequent significant increase of 300% at the station M5 station and 8% in the total nRMS for resistivities >100 Ω.m.
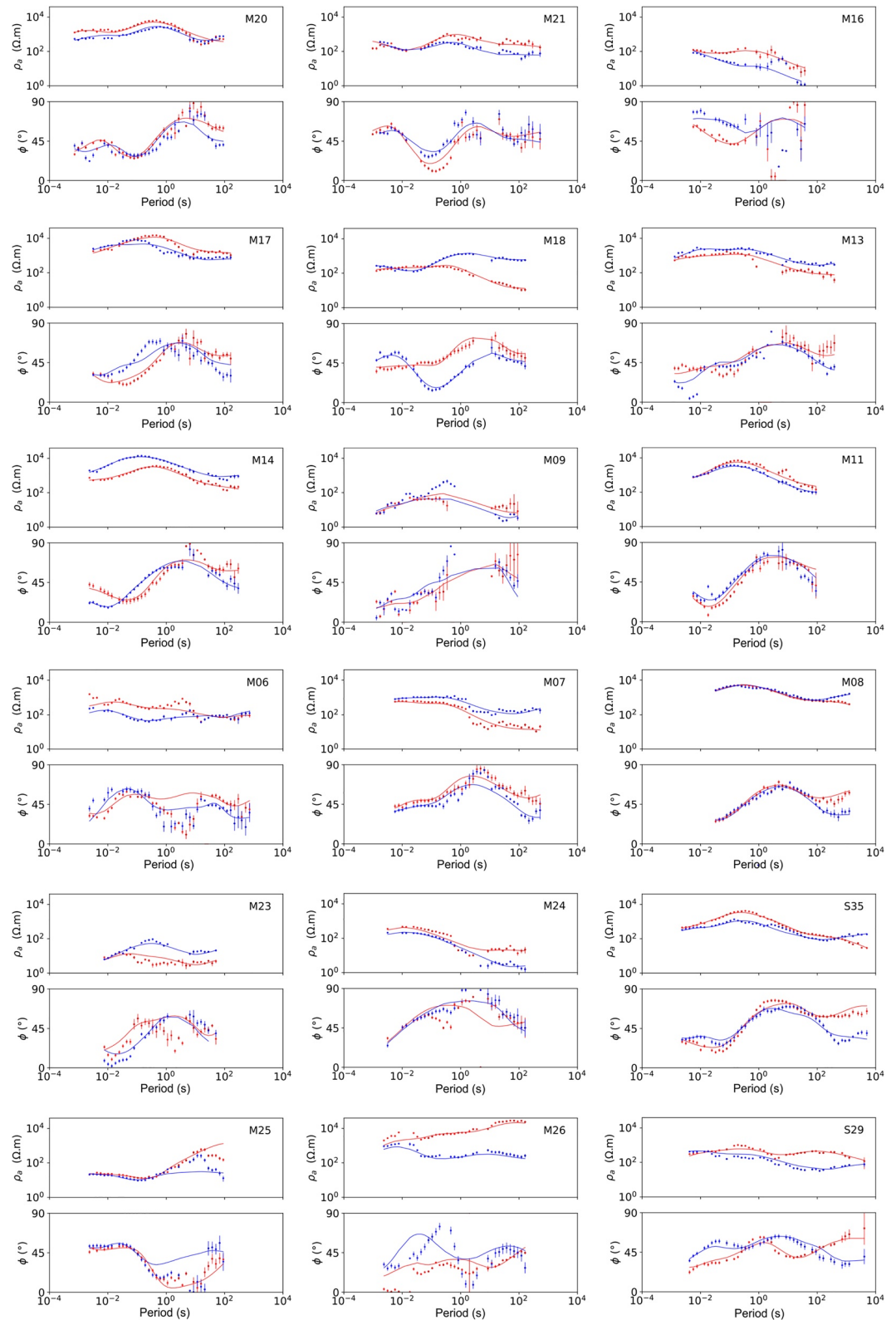
Figure 2. Data fitting from the 3D inversion of all MT stations for an initial model of 1,000 Ω.m. Blue points correspond to the apparent resistivity component $\rho_a yx$ and the red points to the $\rho_a xy$. The model response is highlighted by the colored straight lines (red and blue).
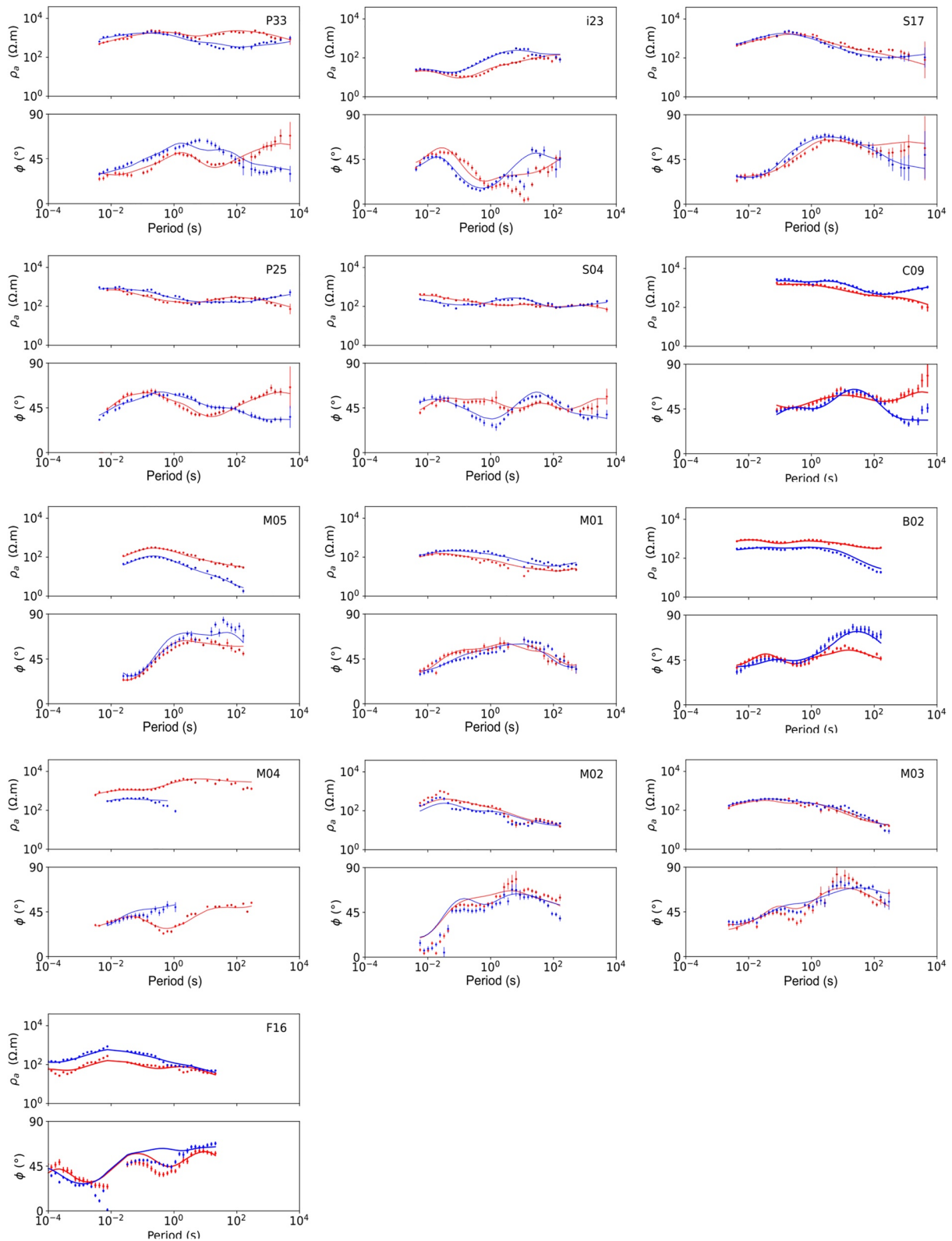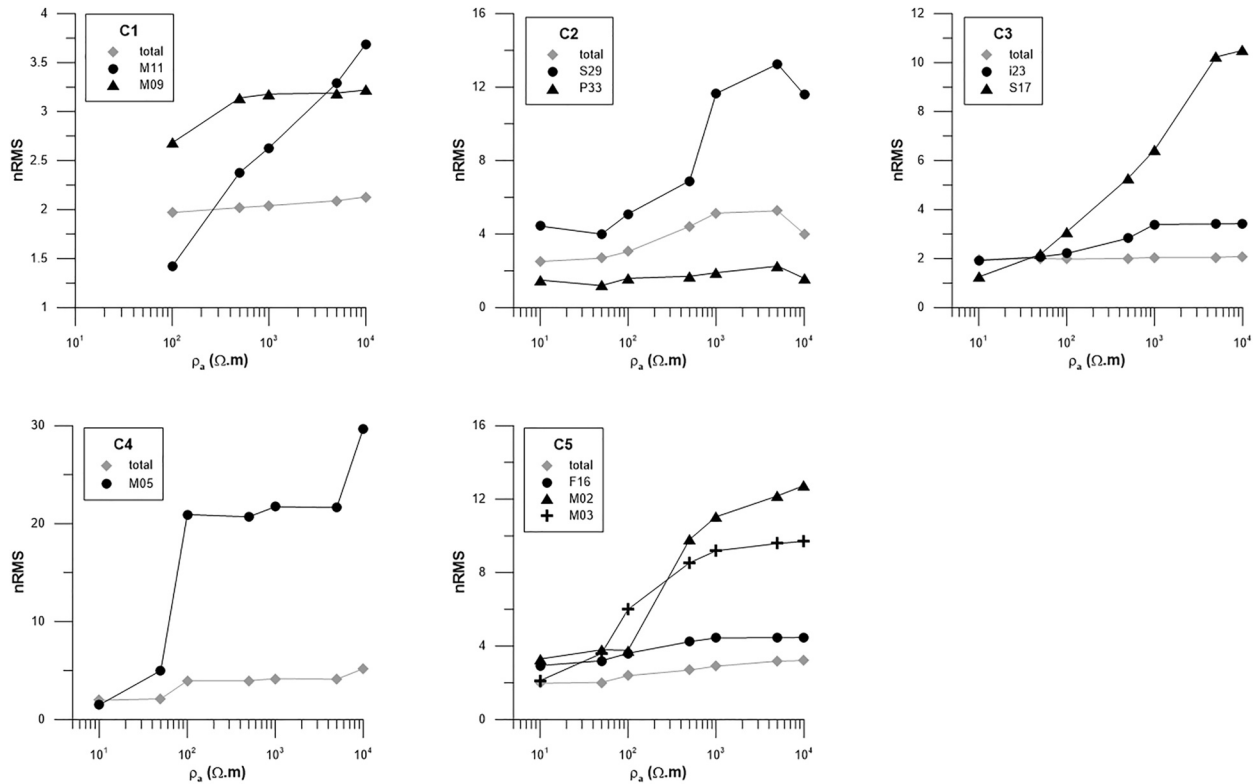
Figure 2. (Continued)

Figure 3. Anomalies Analyses for all conductors (C1, C2, C3, C4, and C5). Each dot represents an nRMS response to a different initial resistivity value (10, 50, 100, 500, 1,000, and 10,000 Ω.m).

The C5 anomaly is detected in three stations, where the changes in resistivity values have a significant impact, especially in stations M2 and M3, affecting the total nRMS value. At station M2, the nRMS values are relatively low for resistivity values <50 Ω.m, with a percentage variation of 20% in nRMS for higher values. At station M3 the behavior of the nRms value is similar but more accentuated, starting to have a considerable variation for resistivities <50 Ω.m with an increase of 114% of the variation in relation to the best mode nRMS. In the total value, the percentage variation for resistivities >50 Ω.m was 21%.

5. Results

The 3D resistivity model of Portugal's mainland is shown by horizontal (Figure 4) and vertical (Figure 5) slices. In general, the crustal segment extending below the central and northern regions of Portugal mainland is much less heterogeneous than its southern counterpart, roughly to the south of TPBCsz, tectonically separating the CIZ from the OMZ. Several resistive (**R1**, **R2**, **R3**) and conductive (**C1**, **C2**, **C3**, **C4**, **C5**) anomalies with different evolution in depth can be observed from north to south.

A large crustal domain of high resistivity (**R1**, from 10^4 to 10^5 Ω.m) extends across the entire GTMZ and a large part of the CIZ, from the surface to a depth of $\approx$17 km (cross-section A to C in Figures 4 and 5) embedded in an area of intermediate resistivity (10^2–10^3 Ω.m). This crustal domain is thicker to the east and becomes thinner westwards. Below, a low resistive anomaly (**C1**, <10^2 Ω.m) at $\approx$17 km depth is roughly resolved (Figure 5, C-C′), which appears to extend westwards at the same depth (Figure 5, profile A-A′). However, the absence of MT stations in profile B-B′ and the low resolution does not allow us to confirm the whole extension of **C1**. A distinct resistive crustal domain **R2** is located in the northern border of OMZ, broadening in depth, where it appears to widen westwards (Figures 4d–4h and 5) along with an increase of the resistivity value (>10^4 Ω.m). A very low resistivity body (**C2**) is imaged by the model between **R1** and **R2**, roughly extending beyond the TPBCsz. The **C2** displays resistivity values between 1 and 50 Ω.m and appears to spread along the TPBCsz until a depth of $\approx$15 km (Figure 5, C-C′ and B-B′).
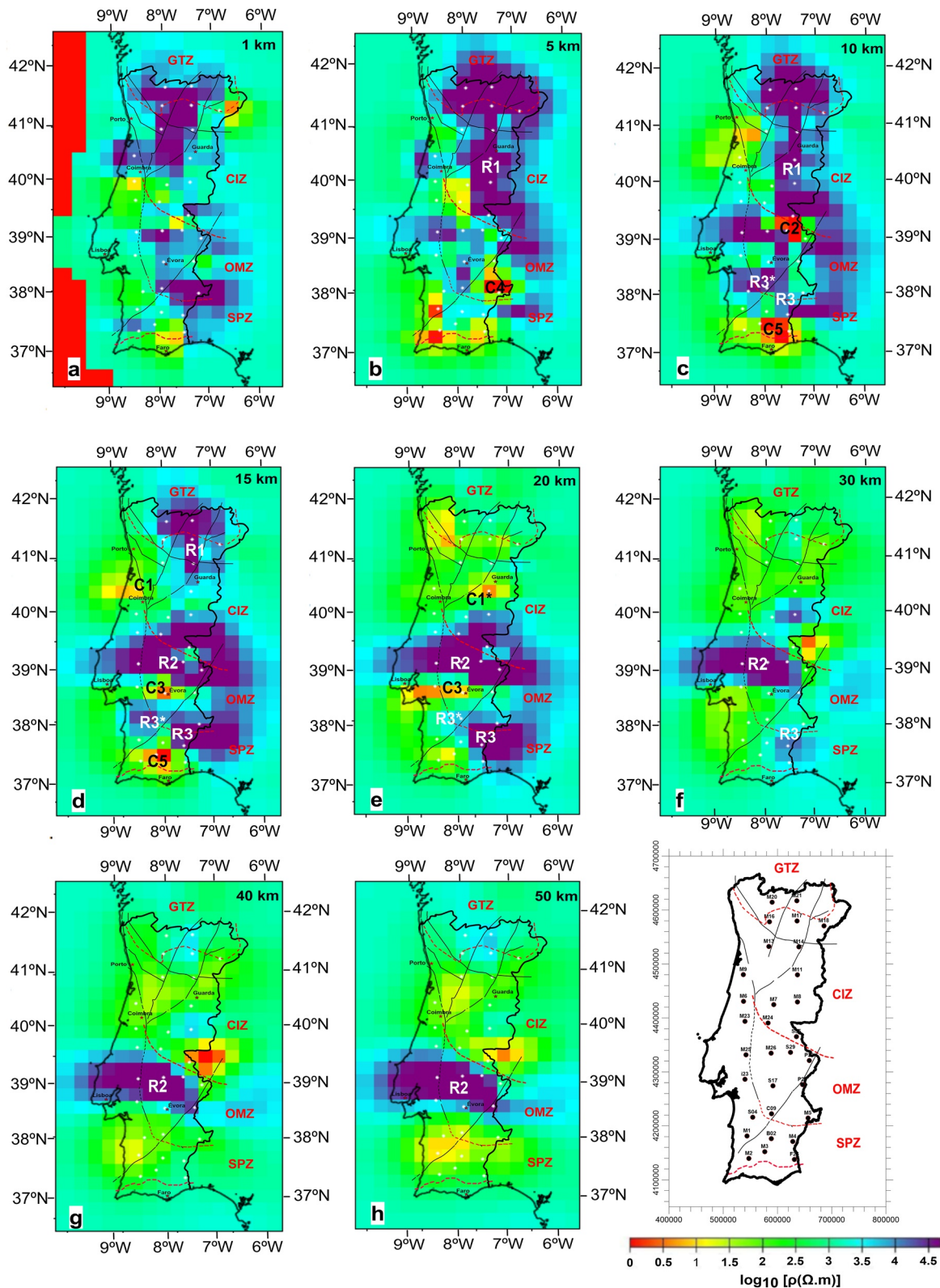
Figure 4. Horizontal slices of the 3D resistivity model for Portugal mainland. Black lines represent the major tectonic structures in the study area (see Figure 1 for reference) and white dots denote the location of the MT soundings. The dashed red lines sign the separation between the main geotectonic units of the Iberian Massif. The resistive and conductive anomalies are labeled with "R" and "C," respectively.
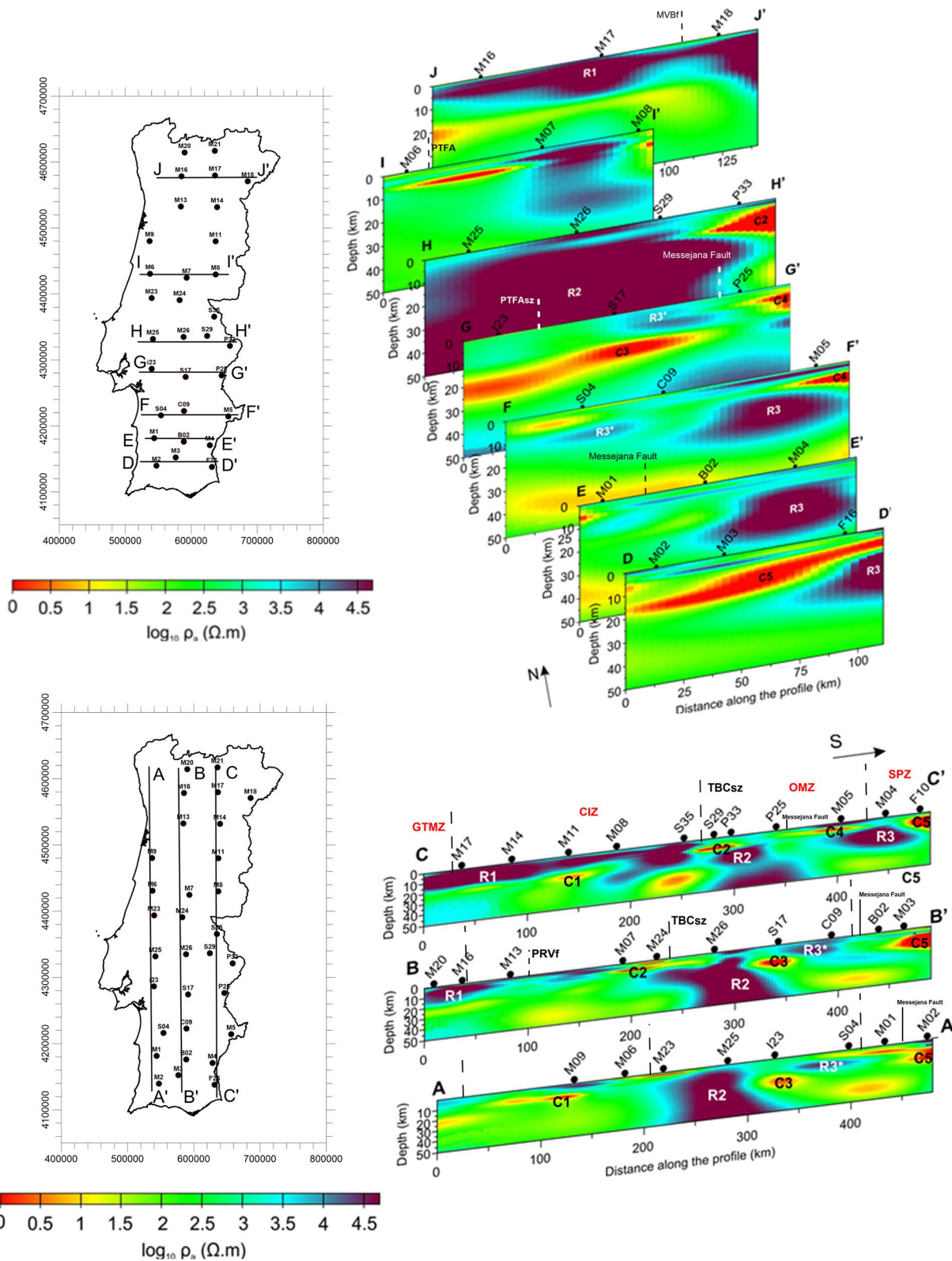
Figure 5. Cross-sections of the 3D resistivity model for Portugal's mainland. The location of MT soundings are indicated by black dots. Top: Cross-sections in W-E direction; Bottom: Cross-sections in N-S direction. The resistive and conductive anomalies are labeled with "R" and "C," respectively.

In the OMZ, another crustal conductive anomaly (**C3**) is unraveled by the computed 3D model, showing resistivity values from 10 to 100 Ω.m. The **C3** extends 30 km along the N-S direction and more than 100 km in the E-W direction (Figures 4d, 4e, and 5, G-G'). This low resistivity crustal domain shows an arched geometry and its possible extension toward the north is obliterated by **R2**. A very high resistive anomaly (**R3**) can be observed to the east-southeast of the Messejana fault zone and from 10 to 23 km depth (Figures 4c–4e and 5). This resistive crustal domain extends across the OMZ-SPZ boundary and further south, spreading over a large part of the latter geotectonic unit (Figures 4c–4f and 5, C-C′). At ≈15 km depth, another resistivity anomaly (**R3***) is imaged to the west of the Messejana fault zone. These two crustal domains show similar resistivity values between 3×10^3 to 4×10^4 Ω.m and are possibly correlated. Below station M05, at a depth of 5 km, a small crustal domain with low resistivity (**C4**) is roughly resolved, displaying values between 10 and 100 Ω.m (Figures 4b and 5, C-C′, F-F′, and G-G'). There is no direct evidence of a connection between **C4** and **C3**; nonetheless, both sit on opposite sides of the Messejana fault zone and have similar resistivity values, possibly implying that they were part of the same crustal domain at some point, further displaced by the fault zone. An area of very low resistivity (**C5**) is detected in the SPZ, ranging from 1 to 50 Ωm. It extends from east to west and displays a bent shape, being shallower on the eastern side (5–10 km depth) and becoming slightly deeper toward the west (20 km depth) (Figures 4c, 4d, and 5, D-D′). In the N-S view (Figure 5, A-A′), **C5** seems to extend northwards, developing a very thin layer beneath the M01 station.

6. Discussion

Results of the computed resistivity model (Figures 4 and 5) indicate that the area extending from 42° to 39.5°N is typified by a significant resistive crustal domain (10^2–10^3 Ω.m) starting at a depth of 15 km, conceivably imaging the high-grade metamorphic crustal rocks beneath the exposed GTMZ Parautochthonous Thrust Complex and CIZ autochthon. This crustal domain is overlain by a higher resistive "cover" (10^4–10^5 Ω.m) that spreads across a wider area, denoting an integrative signal of the high-grade metamorphic rocks forming the Bragança and Morais allochthonous massifs and various Variscan thermal domes, besides the voluminous syn-to late-orogenic granitoid bodies that characterize the GTMZ and CIZ geotectonic units. The difference between these two crustal domains (both composing **R1**) is highlighted in the model by the contrast in resistivity at ≈15 km depth to the east (Figure 5 C-C′), which tends to become shallower to the west as it approaches the PTFAsz (Figures 4 and 5 A-A′, B-B′). This trend is consistent with the spatial distribution of Variscan metamorphic isogrades and of syn-orogenic Variscan granitoids observed in the region, suggesting that the exposed rocks of the CIZ authochthon adjoining PTFAsz represent crustal levels subjected to higher metamorphic grades than those located north-eastwards (Acciaioli, 1997; Bento dos Santos et al., 2021; Ferreira et al., 2019; Valle Aguado et al., 1993). Note also that a significant (up to 2 km) uplift of the PTFAsz eastern block is also consistent with the model results here reported (Figure 5, A-A′, B-B′, and G-G′), notwithstanding the imprecisions imposed by the spacing between the stations (e.g., I23 and S17) and the difficulties in ensuring a straight (and non-controversial) correlation between the resistive domains imaged under these stations.

To the west of PTFAsz the resistive layer is shallower, ≈5 km (Figures 4b, 4c, and 5, A-A′), likely denoting a high-grade metamorphic crustal domain. The range of resistivity values obtained for this crustal domain (10^2–10^3 Ω.m) is similar to that characterizing the lower part of **R1** in CIZ, but also indistinct from the integrative geophysical response of the high-grade Neoproterozoic strip cropping out between Albergaria-a-Velha and Espinho/Porto (to the W of PTFAsz), ascribed to the OMZ in conventional tectonostratigraphic correlations or to the Finisterra Terrane in recent proposals of geodynamic reconstructions (Moreira et al., 2019, and references therein). Accordingly, it is licit to interpret the shallow resistive crustal domain to the west of PTFAsz as an extension in depth of the latter Neoproterozoic strip which present-day exposures are in tectonic contact or partly covered by Meso-Cenozoic sediments.

The PTFAsz is a first order structure in Iberian Massif (e.g., Ribeiro et al., 1990, 2007) but several concerns exist regarding its exact extension to the south (e.g., Arenas et al., 2016; Shelley & Bossiéré, 2000). According to our model, the PTFAsz extends at least to 38°N, 8.5°W (Figures 4 and 5 G-G′, F-F′). A vertical discontinuity with lower resistivity values observed between stations M01 and B02 could be indicative of a further continuation to the south of this major tectonic structure.

The geological meaning of the low resistivity crustal domain **C1** ($<10^2$ Ω.m) at ≈17 km depth is of difficult assessment due to the poor resolution of the model in the face of the lacking of MT stations in profile B-B′. Nevertheless, considering the imaged geometry of **C1** and its positioning in relation to **R1**, it could be tentatively interpreted as a compositional feature of the deep-seated metamorphic rocks forming the mid and lower crustal levels of CIZ. In fact, according to the model results, crustal levels underneath **R1** are consistently typified by intermediate resistivity values, occasionally enclosing higher conductive domains. So, the crustal level in-between **R1** and **C1** could be interpreted as a transitional domain between two crustal sections, the upper one sharing geophysical attributes with the exposed CIZ autochthon, and the lower one displaying a particular rock composition that may justify a generalized decrease in resistivity. Furthermore, considering that we are dealing with the roots of a Paleozoic orogenic belt, the metamorphic rocks forming that lower continental crustal section should be recrystallized under amphibolite to granulite facies conditions and the dissemination of fine-grained, although enough connected, graphite particles may explain the overall decrease in resistivity (e.g., Boerner et al., 1996; Hjelt & Korja, 1993; Monteiro Santos et al., 1999; Monteiro Santos, Mateus, et al., 2002; Monteiro Santos, Matos, et al., 2002; Pous et al., 2004; Wannamaker, 2000). Accepting such interpretation, the variably imaged higher conductive domains within the lower crustal section (like **C1**) may reflect an increase in graphite abundance due to the influence of the primary composition of rocks subjected to prograde metamorphism and/or to the inflow of C-rich fluids into crustal horizons with higher permeability, plausibly related to the development of structural discontinuities (incipient intra-crustal *décollements*).

The crustal domain **R2** is a major feature of the performed resistivity model, steadily extending W-E across the OMZ northern border. In the first 5 km, the contours of **R2** are somewhat diffuse. Nonetheless, it reproduces satisfactorily an array of resistive rocks that could be interpreted as the equivalents in depth of the exposed high-grade metamorphic rocks and granitoid suites of variable morphology and age, affected by a geometrically complex array of tectonic structures related to TPBCsz and PTFAsz. The **R2**-**R1** separation, roughly coinciding with the trace of the TPBCsz, is indicated by a band of consistently lower resistivity values that, enclose a well-defined conductive body (**C2**; Figure 5, B-B′, C-C′). The latter should represent a crustal domain where different tectonic structures merge, therefore incrementing the crustal permeability through the development of fracture-networks of variable density which should have favored the focusing of hydrothermal fluids able to precipitate mineral phases that might increase the rock conductivity (such as sulphides or graphite).

From 15 to 20 km depth, the resistivity contrast of crustal rocks on both sides of the CIZ-OMZ boundary is minor and generates a single resistive crustal domain that also extends reliably to the west, confirming the tendency verified from 10 km depth onwards. This suggests that the imaged crustal section across the CIZ-OMZ boundary at 15–20 km depth is compositionally different from its lateral crustal counterparts to the north and to the south, but similar to the basement rocks sitting beneath the Mesozoic sequences that form the southern part of the Lusitanian Basin. The resistive character of this large crustal domain is compatible with an assortment of high-grade metamorphic rocks and/or granitoid bodies whose spatial distribution has not a straightforward explanation. Using as reference different models of geodynamic reconstruction (e.g., Martínez Catalán et al., 2004, 2019; Mateus et al., 2016; Moreira et al., 2019; Ribeiro et al., 1990, 2007, 2009; Simancas, 2019), that assortment of rocks might include the roots of a Cadomian tectono-metamorphic belt reworked during the Variscan cycle and/or of the deeper crustal sections of the Finisterra Terrane. However, this possible interpretation does not explain why **R2** became clearly defined after 30 km depth, spreading from 39.5° to 38.5°N and apparently bounded to the east by the Messejana fault zone. Accordingly, we are forced to conclude that the lower crust/upper mantle section beneath a significant part of the northern OMZ and southern Lusitanian Basin is inherently resistive, comprising rock associations distinct from those included in contiguous equivalent lithospheric sections.

The high resistivity anomaly **R3-R3***, observed from the first kilometer to ≈30 km depth, spreads over the OMZ-SPZ boundary and the NE part of the SPZ northern border, providing an integrative signal of distinct resistive crustal domains. In the initial ≈5 km depth, the **R3-R3*** (in particular the latter) is basically confined to the deeper extensions of granites that intrude the Pulo do Lobo Terrane and of resistive geological formations shaping the OMZ Southern Crystalline belt (such as the Beja Igneous Complex and the Évora granite massif), besides the Beja-Acebuches Ophiolite Complex and several preserved remnants of Neoproterozoic metamorphic successions. At about 5 km depth, the **R3-R3*** anomaly is detached by a conductive body (**C4**), which reinforces a possible displacement imposed by the Messejana fault zone. However, the resistive signal persists afterward, namely until a deepness of ≈20 km, even though the irregular fading and possible dismembering of

R3* toward depth. The concurrent strengthening of **R3** at 20 km depth and its clear tendency to E-ESE shifting until disappears at 30 km depth, suggests that the imaged resistive character of this lower crustal section is due to deep-seated high grade metamorphic rocks composing the tectonically amalgamated basement beneath the Pulo do Lobo Terrane and the adjoining SPZ.

The conductive body **C4**, possibly displaced by the Messejana fault zone, represents a crustal domain similar to that imaged by **C3**, placed at ≈15 km depth (Figure 5 G-G′). These mid-crust conductors were already recognized in previous studies with similar resistivity values (e.g., Muñoz et al., 2008; Vieira da Silva et al., 2007), and differences in spatial extension could merely denote distinct model resolutions. As comprehensively discussed in Monteiro Santos, Mateus, et al. (2002), Monteiro Santos, Matos, et al. (2002), and Muñoz et al. (2008), the development of these low resistivity bodies could be interpreted as a result of interconnected graphite in structural discontinuities that compose a regional mid-crustal *décollement* at ≈ 13–15 km depth. Similarly, the very large, E-W low resistivity crustal domain **C5** imaged in SPZ should represent a deep-seated major *décollement* where some main (reactivated) thrust zones recognized along the SPZ-Algarve Basin boundary might be enrooted (e.g., Terrinha, 1998). In this regard note that **C5** lies at a depth of 15–20 km to the west and of 10–15 km to the east, and does not spread significantly to the north, although it prolongs markedly eastwards.

Some cross-sections suggest a possible connection between **C5** and a more superficial conductor beneath station M01 (e.g., Figure 5 A-A′). This could be an artifact of the performed MT data inversion, considering also the large spacing between MT stations. Even so, the situation imaged by station M01 could simply represent a tectonic ramp of a deeper thrust zone despite the possible disturbance caused by the Messejana fault zone. This interpretation is geometrically consistent with the structural arrays that characterize the tectonic stacking observed in several sections of the Iberian Pyrite Belt to the East of the Messejana fault zone (Inverno et al., 2015 and references therein; Matos et al., 2020), being also compatible with the general architecture proposed for the SPZ, a syn-orogenic foreland belt.

7. Conclusion

The magnetotelluric method provides useful data to unravel the architecture and composition of hidden crustal domains. The reported data support the first 3D resistivity model covering the entire Portuguese mainland, allowing the delineation of multiple resistive and conductive crustal domains with significant deep and lateral extension.

The main resistivity anomalies identified from north to south are: **R1**, a relatively shallow (down to ≈17 km) resistive crustal domain (10^4 to 10^5 Ω.m) spreading across the GTMZ and CIZ tectonic units, possibly related to the voluminous sin-to late-orogenic granitoid bodies and high-grade metamorphic rocks that characterize these units; **R2**, a deep resistive (>10^4 Ω.m) crustal domain, down to at least 50 km and extending W-E across the OMZ northern border, likely corresponding to a deep equivalent of the exposed high-grade metamorphic rocks bounded by the TPBCsz and PTFAsz shear zones; **R3-R3*** with resistivity values of 3×10^3 - 4×10^4 Ω.m and at depths from 10 to 30 km, spreading over the OMZ-SPZ boundary, located on one side and the other of the Messejana fault zone, and possibly representing the deeper extensions of the voluminous igneous bodies intruding this region (such as the Beja Igneous Complex and the Évora granite massif).

The main conductive anomalies detected, also from north to south, are the following: **C1**, at ≈17 km depth and below **R1**, with resistivity <10^2 Ω.m, possibly related with the dissemination of connected fine-grained graphite particles; **C2**, a conductive crustal domain (1–50 Ω.m) at 10–15 km depth, roughly coinciding with the TPBCsz and separating the resistive domains **R1** and **R2**; **C3**, at ≈15 km depth and with resistivity values of 1–100 Ω.m, delimiting a W-E crustal domain in the OMZ, identified in previous studies using MT data and interpreted as the result of interconnected graphite in structural discontinuities; **C4**, possibly displaced by the Messejana fault zone, and representing a crustal domain similar to **C3**, located at ≈15 km depth and exhibiting resistivity values of 10–100 Ω.m; **C5**, a very large W-E crustal domain in the SPZ at a greater depth in the west (15–20 km) than in the east (10–15 km) and with resistivity values of 1–50 Ω.m, likely related to the roots of well-known thrust zones along the boundary between the SPZ and the Algarve Basin.

The subsurface image obtained from MT methods is consistent with existing geological information on the Portugal mainland region and, in some cases, it brings new possible answers to unsolved problems. It should

be emphasized that the work presented here provides the basis for future improvements to the 3D resistivity model for Portugal mainland. The results obtained have already provided contributions to the hazard assessment related to geomagnetically induced currents (GICs) in the Portuguese power transmission network (Alves Ribeiro et al., 2021; Baltazar-Soares et al., 2021). Considering the wide frequency spectrum of geomagnetic storms that can cause disturbances in power lines, long-period MT soundings should be conducted in the future to increase the resolution of the results available so far.

Data Availability Statement

Data from 10 MT soundings in the southern region of Portugal, carried out between 1997 and 2002, are attributed to Almeida et al. (2001, 2005), Pous et al. (2004), and Alves Ribeiro et al. (2017). The remaining data from 21 MT stations collected during this study are available at Baltazar-Soares et al. (2022).

References

Acciaioli, M. H. (1997). *Processos metamórficos variscos na Serra da Freita (Zona Centro Ibérica, Portugal)* (Tese de Doutoramento). Universidade de Aveiro.

Almeida, E., Monteiro Santos, F. A., Mateus, A., Heise, W., & Pous, J. (2005). Magnetotelluric measurements in SW Iberia: New data for the Variscan crustal structures. *Geophysical Research Letters*, *32*(8), L08312. https://doi.org/10.1029/2005GL022596

Almeida, E., Pous, J., Santos, F. M., Fonseca, P., Marcuello, A., Queralt, P., et al. (2001). Electromagnetic imaging of a transpressional tectonics in SW Iberia. *Geophysical Research Letters*, *28*(3), 439–442. https://doi.org/10.1029/2000GL012037

Alves Ribeiro, J. (2018). *Magnetotelluric studies in detecting an old suture zone and major crustal scale shear zones (Iberia)* (PhD dissertation). Universidade de Lisboa.

Alves Ribeiro, J., Monteiro-Santos, F. A., Pereira, M. F., Díez Fernández, R., Dias da Silva, Í., Nascimento, C., & Silva, J. B. (2017). Magnetotelluric imaging of the lithosphere across the Variscan Orogen (Iberian autochthonous domain, NW Iberia). *Tectonics*, *36*(12), 3065–3080. https://doi.org/10.1002/2017TC004593

Alves Ribeiro, J., Pinheiro, F. J. G., & Pais, M. A. (2021). First estimations of geomagnetically induced currents in the South of Portugal. *Space Weather*, *19*(1), e2020SW002546. https://doi.org/10.1029/2020SW002546

Amante, C., & Eakins, B. W. (2009). *ETOPO1 1 arc-minute global relief model: Procedures, data sources and analysis. NOAA Technical Memorandum NESDIS NGDC-24*. National Geophysical Data Center. NOAA 10 (2009): V5C8276M.

Arenas, R., Díez Fernández, R., Rubio Pascual, F. J., Sánchez Martínez, S., Martín Parra, L. M., Matas, J., et al. (2016). The Galicia–Ossa-Morena Zone: Proposal for a new zone of the Iberian Massif. Variscan implications. *Tectonophysics*, *681*, 135–143. https://doi.org/10.1016/j.tecto.2016.02.030

Arroucau, P., Custódio, S., Civiero, C., Silveira, G., Dias, N., Díaz, J., et al. (2021). PRISM3D: A 3-D reference seismic model for Iberia and adjacent areas. *Geophysical Journal International*, *225*(2), 789–810. https://doi.org/10.1093/gji/ggab005

Arthaud, F., & Matte, P. (1975). Les décrochements Tardi-Hercyniens du Sudoest de l'Éurope. Géometrie et essai de reconstituition de la défórmation. *Tectonophysics*, *25*(1–2), 139–171. https://doi.org/10.1016/0040-1951(75)90014-1

Azor, A., Dias da Silva, Í., Gómez Barreiro, J., González-Clavijo, E., Martínez Catalán, J. R., Simancas, J. F., et al. (2019). Deformation and structure. In C. Quesada & J. T. Oliveira (Eds.), *[Regional Geology Reviews] The Geology of Iberia: A Geodynamic Approach*, *The Variscan Cycle, Chapter 10* (Vol. 2, pp. 307–348). https://doi.org/10.1007/978-3-030-10519-8

Bai, D., Unsworth, M. J., Meju, M. A., Ma, X., Teng, J., Kong, X., et al. (2010). Crustal deformation of the eastern Tibetan plateau revealed by magnetotelluric imaging. *Nature Geoscience*, *3*(5), 358–362. https://doi.org/10.1038/ngeo830

Baltazar-Soares, P., Martinez Moreno, F., Alves Ribeiro, J., Monteiro Santos, F., Pais, M. A., & Ribeiro, P. (2021). Crustal characterization of Portugal´s mainland based on Magnetotelluric measurements. In *EGU General Assembly Conference Abstracts* (pp. EGU21–15690). https://doi.org/10.5194/egusphere-egu21-15690

Baltazar-Soares, P., Martinez Moreno, F., Alves Ribeiro, J., Monteiro Santos, F., Pais, M. A., Ribeiro, P., et al. (2022). Project MAG-GIC (PTDC/CTA-GEO/31744/2017). Crustal Characterization of Portugal´s mainland based on Magnetotelluric measurements [Dataset]. Zenodo. https://doi.org/10.5281/zenodo.7147543

Bento dos Santos, T., Rodrigues, J. F., Castro, P., Cotrim, B., Pereira, I., Ferreira, J. A., et al. (2021). Exhumation of an anatectic complex by channel flow and extrusion tectonics: Structural and metamorphic evidence from the Porto–Viseu Metamorphic Belt, Central-Iberian Zone. *International Journal of Earth Sciences*, *110*(6), 2179–2201. https://doi.org/10.1007/s00531-021-02067-z

Berdichevsky, M. N. (1960). Principles of magnetotelluric profiling theory. *Applied Geophysics*, *28*, 70–91.

Boerner, D. E., Kurtz, R. D., & Craven, J. A. (1996). Electrical conductivity and Paleo-Proterozoic foredeeps. *Journal of Geophysical Research*, *101*(B6), 13775–13791. https://doi.org/10.1029/96jb00171

Cagniard, L. (1953). Basic theory of the magneto-telluric method of geophysical prospecting. *Geophysics*, *18*(3), 605–635. https://doi.org/10.1190/1.1437915

Cebriá, J. M., López-Ruiz, J., Doblas, M., Martins, L. T., & Munhá, J. (2003). Geochemistry of the Early Jurassic Messejana-Placencia dyke (Portugal–Spain); implications on the origin of the Central Atlantic Magmatic Province. *Journal of Petrology*, *44*(3), 547–568. https://doi.org/10.1093/petrology/44.3.547

Corseri, R., Senger, K., Selway, K., Abdelmalak, M. M., Planke, S., & Jerram, D. A. (2017). Magnetotelluric evidence for massive sulphide mineralization in intruded sediments of the outer Vøring Basin, mid-Norway. *Tectonophysics*, *706–707*, 196–205. https://doi.org/10.1016/j.tecto.2017.04.011

Da Silva, I. D., Linnemann, U., Hofmann, M., Gonzalez-Clavijo, E., Diez-Montes, A., & Martinez Catalan, J. R. (2015). Detrital zircon and tectonostratigraphy of the Parautochthon under the Morais Complex (NE Portugal): Implications for the Variscan accretionary history of the Iberian Massif. *Journal of the Geological Society*, *172*(1), 45–61. https://doi.org/10.1144/jgs2014-005

Dias, R., & Ribeiro, A. (1995). The Ibero-Armorican Arc: A collision effect against an irregular continent? *Tectonophysics*, *246*(1–3), 113–128. https://doi.org/10.1016/0040-1951(94)00253-6

Dias Da Silva, Í., Valverde-Vaquero, P., González-Clavijo, E., Díez-Montes, A., & Martínez Catalán, J. R. (2014). Structural and stratigraphical significance of U–Pb ages from the Mora and Saldanha volcanic complexes (NE Portugal, Iberian Variscides). *Geological Society, London, Special Publications*, *405*(1), 115–135. https://doi.org/10.1144/sp405.3

Dündar, S., Dias, N. A., Silveira, G., Kind, R., Vinnik, L., Matias, L., & Bianchi, M. (2016). Estimation of the crustal bulk properties beneath Mainland Portugal from P-wave teleseismic receiver functions. *Pure and Applied Geophysics*, *173*(6), 1949–1970. https://doi.org/10.1007/s00024-016-1257-4

Egbert, G. D., & Booker, J. R. (1986). Robust estimation of geomagnetic transfer functions. *Geophysical Journal of the Royal Astronomical Society*, *87*(1), 173–194. https://doi.org/10.1111/j.1365-246x.1986.tb04552.x

Egbert, G. D., & Kelbert, A. (2012). Computational recipes for electromagnetic inverse problems. *Geophysical Journal International*, *189*(1), 251–267. https://doi.org/10.1111/j.1365-246X.2011.05347.x

Farzamian, M., Alves Ribeiro, J., Khalil, M. A., Monteiro Santos, F. A., Filbandi Kashkouli, M., Bortolozo, C. A., & Mendonça, J. L. (2018). Application of transient electromagnetic and audio-magnetotelluric methods for imaging the Monte real aquifer in Portugal. *Pure and Applied Geophysics*, *176*(2), 719–735. https://doi.org/10.1007/s00024-018-2030-7

Ferreira, J. A., Bento dos Santos, T., Pereira, I., & Mata, J. (2019). Tectonically assisted exhumation and cooling of Variscan granites in an anatectic complex of the Central Iberian Zone, Portugal: Constraints from LA-ICP-MS zircon and apatite U-Pb ages. *International Journal of Earth Sciences*, *108*(7), 2153–2175. https://doi.org/10.1007/s00531-019-01755-1

Figueiras, J., Mateus, A., Gonçalves, M. A., Waerenborgh, J. C., & Fonseca, P. (2002). Geodynamic evolution of the South Variscan Iberian Suture as recorded by mineral transformations. *Geodinamica Acta*, *15*(1), 45–61. https://doi.org/10.1080/09853111.2002.10510738

González-Castillo, L., Galindo-Zaldívar, J., Junge, A., Martínez-Moreno, F. J., Löwer, A., de Galdeano, C. S., et al. (2015). Evidence of a large deep conductive body within the basement of the Guadalquivir foreland Basin (Betic Cordillera, S-Spain) from tipper vector modelling: Tectonic implications. *Tectonophysics*, *663*, 354–363. https://doi.org/10.1016/j.tecto.2015.08.013

Graham, H., Jingming, D., Alison, K., Kate, R., Stephan, T., Sasha, A., & Wolfgang, S. (2021). Lower crustal resistivity signature of an orogenic gold system. *Scientific Reports*, *11*(1), 15807. https://doi.org/10.1038/s41598-021-94531-8

Gutiérrez-Marco, J. C., Piçarra, J. M., Meireles, C. A., Cózar, P., García-Bellido, D. C., Pereira, Z., et al. (2019). Early Ordovician–Devonian passive margin stage in the Gondwanan units of the Iberian Massif. In C. Quesada & J. Oliveira (Eds.), *The Geology of Iberia: A Geodynamic Approach. Regional Geology Reviews*. Springer. https://doi.org/10.1007/978-3-030-10519-8_3

Hjelt, S.-E., & Korja, T. (1993). Lithospheric and upper-mantle structures, results of electromagnetic soundings in Europe. *Physics of the Earth and Planetary Interiors*, *79*(1–2), 137–177. https://doi.org/10.1016/0031-9201(93)90146-z

Inverno, C., Díez-Montes, A., Rosa, C., García-Crespo, J., Matos, J., García-Lobón, J. L., et al. (2015). Introduction and geological setting of the Iberian Pyrite Belt. *3D, 4D and predictive modelling of major mineral belts in Europe* (pp. 191–208). https://doi.org/10.1007/978-3-319-17428-0_9

Julivert, M., Fontboté, J., Ribeiro, A., & Conde, L. (1972). *Mapa Tectónico de la Península Ibérica Y Baleares. 1:1 000 000* (p. 113). Instituto Geológico Y Minero de España.

Julivert, M., Fontboté, J. M., Ribeiro, A., & Conde, L. E. (1974). *Mapa Tectónico de la Península Ibérica y Baleares (Tectonic map of the Iberian Peninsula and Baleárian Ilands)* (p. 113). IGME-SPI, Instituto Geológico y Minero de España.

Kelbert, A., Meqbel, N., Egbert, G. D., & Tandon, K. (2014). ModEM: A modular system for inversion of electromagnetic geophysical data. *Computers & Geosciences*, *66*, 40–53. https://doi.org/10.1016/j.cageo.2014.01.010

Lotze, F. (1945). Zur Gliederung der Varisziden der Iberischen Meseta. *Geotekton Forschg.*, *6*, 78–92.

Marques, F. O., Mateus, A., & Tassinari, C. (2002). The Late-Variscan fault network in central-northern Portugal. *Tectonophysics*, *359*(3–4), 255–270. https://doi.org/10.1016/S0040-1951(02)00514-0

Martínez-Catalán, J. R., Aller, J., Alonso, J. L., & Bastida, F. (2009). *The Iberian Variscan orogeny, Spanish Geological Frameworks and Geosites: An approach to Spanish Geological Heritage of International Relevance* (pp. 978–984). IGME.

Martínez Catalán, J. R., Gómez Barreiro, J., Dias da Silva, Í., Chichorro, M., López-Carmona, A., Castiñeiras, P., et al. (2019). Variscan suture zone and suspect terranes in the NW Iberian Massif: Allochthonous complexes of the Galicia-Trás os Montes Zone (NW Iberia). In C. Quesada & J. T. Oliveira (Eds.), *The Geology of Iberia: A geodynamic approach: Volume 2: The Variscan Cycle* (pp. 99–130). Springer International Publishing. https://doi.org/10.1007/978-3-030-10519-8_4

Martínez Catalán, J. R., Martínez Poyatos, D., & Bea, F. (2004). Zona Centro Ibérica (coords.). In J. A. Vera (Ed.), *Gelogia de España* (pp. 68–133). SGE-IGME.

Martínez-Catalán, J. R., Rubio Pascual, F. J., Montes, A. D., Fernández, R. D., Barreiro, J. G., Dias da Silva, Í., et al. (2014). The late Variscan HT/LP metamorphic event in NW and Central Iberia: Relationships to crustal thickening, extension, orocline, development and crustal evolution. *Geological Society, London, Special Publications*, *405*(1), 225–247. https://doi.org/10.1144/SP405.1

Martins, L. T. (1991). *Actividade Ígnea Mesozóica em Portugal* (PhD). Universidade de Lisboa.

Mateus, A., Figueiras, J., Gonçalves, M. A., & Fonseca, P. (1999). Evolving fluid circulation within the Variscan Beja-Acebuches Ophiolite Complex (SE, Portugal). *Ofioliti*, *24*(2), 269–282. https://doi.org/10.4454/ofioliti.v24i2.107

Mateus, A., Munhá, J., Ribeiro, A., Tassinari, C. C. G., Sato, K., Pereira, E., & Santos, J. F. (2016). U-Pb SHRIMP zircon dating of high-grade rocks from the Upper Allochthonous Terrane of Bragança and Morais Massifs (NE Portugal); geodynamic consequences. *Tectonophysics*, *675*, 23–49. https://doi.org/10.1016/j.tecto.2016.02.048

Matos, J. X., Carvaho, J., & Represas, P. (2020). Geophysical surveys in the Portuguese sector of the Iberian Pyrite Belt: A global overview focused on the massive sulphide exploration and geologic interpretation. *Comunicações Geológicas*, *107*(3), 41–78.

Meqbel, N. M., Egbert, G. D., Wannamaker, P. E., Kelbert, A., & Schultz, A. (2014). Deep electrical resistivity structure of the northwestern US derived from 3-D inversion of USArray magnetotelluric data. *Earth and Planetary Science Letters*, *402*, 290–304. https://doi.org/10.1016/j.epsl.2013.12.026

Miensopust, M. P. (2017). Application of 3-D electromagnetic inversion in practice: Challenges, pitfalls and solution approaches. *Surveys in Geophysics*, *38*(5), 869–933. https://doi.org/10.1007/s10712-017-9435-1

Monteiro Santos, F. A., Dupis, A., Andrade Afonso, A. R., & Mendes-Victor, L. A. (1995). Magnetotelluric observations over the Chaves geothermal field (NE Portugal)—Preliminary results. *Physics of the Earth and Planetary Interiors*, *91*(4), 203–211. https://doi.org/10.1016/0031-9201(95)03066-6

Monteiro Santos, F. A., Mateus, A., Almeida, E. P., Pous, J., & Mendes-Victor, L. A. (2002). Are some of the deep crustal conductive features found in SW Iberia caused by graphite? *Earth and Planetary Science Letters*, *201*(2), 353–367. https://doi.org/10.1016/S0012-821X(02)00721-5

Monteiro Santos, F. A., Matos, L., Almeida, E., Mateus, A., Matias, H., & Mendes-Victor, L. A. (2002). Three-dimensional magnetotelluric modelling of the Vilariça depression (NE Portugal). *Journal of Applied Geophysics*, *49*(1–2), 59–74. https://doi.org/10.1016/S0926-9851(01)00099-4

Monteiro Santos, F. A., Pous, J., Almeida, E. P., Queralt, P., Marcuello, A., Matias, H., & Mendes Victor, L. A. (1999). Magnetotelluric survey of the electrical conductivity of the crust across the Ossa Morena Zone and South Portuguese Zone suture. *Tectonophysics*, *313*(4), 449–462. https://doi.org/10.1016/S0040-1951(99)00209-7

Monteiro Santos, F. A., Soares, A., Nolasco, R., Rodrigues, H., Luzio, R., Palshin, N., & ISO-3D team (2003). Lithosphere conductivity structure using the CAM-1 (Lisbon-Madeira) submarine cable. *Geophysical Journal International*, *155*(2), 591–600. https://doi.org/10.1046/j.1365-246X.2003.02060.x

Moreira, N., Romão, J., Dias, R., Ribeiro, A., & Pedro, J. (2019). The Finisterra-Léon-Mid German Cristalline Rise Domain; Proposal of a New Terrane in the Variscan Chain. In C. Quesada & J. Oliveira (Eds.), *The Geology of Iberia: A Geodynamic Approach*. *Regional Geology Reviews*. Springer. https://doi.org/10.1007/978-3-030-10519-8_7

Muñoz, G., Heise, W., Paz, C., Almeida, E., Monteiro Santos, F. A., & Pous, J. (2005). New magnetotelluric data trough the boundary between the Ossa Morena and Centroiberian Zones. *Geológica Acta*, *3*, 215–223.

Muñoz, G., Mateus, A., Pous, J., Heise, W., Monteiro Santos, F., & Almeida, E. (2008). Unraveling middle-crust conductive layers in Paleozoic Orogens through 3D modeling of magnetotelluric data: The Ossa-Morena Zone case study (SW Iberian Variscides). *Journal of Geophysical Research*, *113*(B6), B06106. https://doi.org/10.1029/2007JB004978

Oliveira, J. T., González-Clavijo, E., Alonso, J., Armendáriz, M., Bahamonde, J. R., Braid, J. A., et al. (2019). Synorogenic Basins. In C. Quesada & J. Oliveira (Eds.), *The Geology of Iberia: A Geodynamic Approach*. *Regional Geology Reviews*. Springer. https://doi.org/10.1007/978-3-030-10519-8_11

Oliveira, J. T., Quesada, C., Pereira, Z., Matos, J. X., Solá, A. R., Rosa, D., et al. (2019). South Portuguese terrane: A continental affinity exotic unit. In C. Quesada & J. Oliveira (Eds.), *The Geology of Iberia: A Geodynamic Approach*. *Regional Geology Reviews*. Springer. https://doi.org/10.1007/978-3-030-10519-8_6

Pous, J., Muñoz, G., Heise, W., Melgarejo, J. C., & Quesada, C. (2004). Electromagnetic imaging of Variscan crustal structures in SW Iberia: The role of interconnected graphite. *Earth and Planetary Science Letters*, *217*(3–4), 435–450. https://doi.org/10.1016/S0012-821X(03)00612-5

Prodehl, C., Moreira, V. S., Mueller, S., & Mendes, A. S. (1975). Deep-seismic sounding experiments in central and southern Portugal. In *General Assembly of the European Seismological Commission (14th – Berlin)* (pp. 261–266).

Quesada, C., Braid, J. A., Fernandes, P., Ferreira, P., Jorge, R. S., Matos, J. X., et al. (2019). SW Iberia Variscan Suture Zone: Oceanic affinity units. In C. Quesada & J. Oliveira (Eds.), *The Geology of Iberia: A Geodynamic Approach*. *Regional Geology Reviews*. Springer. https://doi.org/10.1007/978-3-030-10519-8_5

Quesada, C., Fonseca, P. E., Munhá, J., Oliveira, J. T., & Ribeiro, A. (1994). The Beja-Acebuches Ophiolite (Southern Iberia Variscan fold belt): Geological characterization and geodynamic significance. *Boletin Geologico y Minero*, *105*(1), 3–49.

Ramos, A., Fernández, O., Terrinha, P., & Muñoz, J. (2016). Extension and inversion structures in the Tethys–Atlantic linkage zone, Algarve Basin, Portugal. *International Journal of Earth Sciences*, *105*(5), 1663–1679. https://doi.org/10.1007/s00531-015-1280-1

Ribeiro, A. (1974). Contribution à l'étude tectonique de Trás-os-Montes Oriental. *Mem. Serv. Geol. Portugal*, *24*, 168.

Ribeiro, A. (1981). A geotransverse through the Variscan fold belt in Portugal. In H. J. Zwart & V. F. Dornsiepen (Eds.), *The Variscan Orogen in Europe*, *Geologie en Mijnbouw* (Vol. 60, pp. 41–44).

Ribeiro, A., Antunes, M. T., Ferreira, M. P., Rocha, R. B., Soares, A.-F., Zbyszewski, G., et al., (1979). *Introduction a la Geologic Generale do Portugal*. Serviços Geológicos de Portugal (p. 114). https://doi.org/10.1016/0040-1951(90)90448-h

Ribeiro, A., Munhá, J., Dias, R., Mateus, A., Pereira, E., Ribeiro, L., et al. (2007). Geodynamic evolution of the SW Europe Variscides. *Tectonics*, *26*(6), TC6009. https://doi.org/10.1029/2006tc002058

Ribeiro, A., Munhá, J., Fonseca, P. E., Araújo, A., Pedro, J. C., Mateus, A., et al. (2010). Variscan ophiolite belts in the Ossa-Morena Zone (Southwest Iberia): Geological characterization and geodynamic significance. *Gondwana Research*, *17*(2–3), 408–421. https://doi.org/10.1016/j.gr.2009.09.005

Ribeiro, A., Munhá, J., Mateus, A., Fonseca, P., Pereira, E., Noronha, F., et al. (2009). Mechanics of thick-skinned Variscan overprinting of Cadomian basement (Iberian Variscides). *Comptes Rendus Geoscience*, *341*(2–3), 127–139. https://doi.org/10.1016/j.crte.2008.12.003

Ribeiro, A., Quesada, C., & Dallmeyer, R. D. (1990). Geodynamic evolution of the Iberian Massif. In R. D. Dallmeyer & E. Martínez García (Eds.), *Pre-Mesozoic Geology of Iberia* (pp. 399–409). Springer-Verlag. https://doi.org/10.1007/978-3-642-83980-1_28

Ribeiro, M. L., Castro, A., Almeida, A., González Menéndez, L., Jesus, A., Lains, J. A., et al. (2019). Variscan magmatism. In C. Quesada & J. Oliveira (Eds.), *The Geology of Iberia: A Geodynamic Approach*. *Regional Geology Reviews*. Springer. https://doi.org/10.1007/978-3-030-10519-8_13

Ribeiro, M. L., Reche, J., López-Carmona, A., Aguilar, C., Bento dos Santos, T., Chichorro, M., et al. (2019). Variscan metamorphism. In C. Quesada & J. Oliveira (Eds.), *The Geology of Iberia: A Geodynamic Approach*. *Regional Geology Reviews*. Springer. https://doi.org/10.1007/978-3-030-10519-8_12

Sánchez-García, T., Chichorro, M., Solá, A. R., Álvaro, J. J., Diéz-Montes, A., Bellido, F., et al. (2019). The Cambrian-Early Ordovician Rift stage in the Gondwanan Units of the Iberian Massif. In C. Quesada & J. Oliveira (Eds.), *The Geology of Iberia: A Geodynamic Approach*. *Regional Geology Reviews*. Springer. https://doi.org/10.1007/978-3-030-10519-8_2

Shelley, D., & Bossieré, G. (2000). A new model for the Hercynian Orogen of Gondwanan France and Iberia. *Journal of Structural Geology*, *22*(6), 757–776. https://doi.org/10.1016/s0191-8141(00)00007-9

Silva, P. F., Henry, B., Marques, F. O., Font, E., Mateus, A., Vegas, R., et al. (2008). Magma flow, exsolution processes and rock metasomatism in the Great Messejana-Plasencia dyke (Iberian Peninsula). *Geophysical Journal International*, *175*(2), 806–824. https://doi.org/10.1111/j.1365-246x.2008.03920.x

Simancas, J. F. (2019). Variscan Cycle. In C. Quesada & J. T. Oliveira (Eds.), *[Regional Geology Reviews] The Geology of Iberia: A Geodynamic Approach (Volume 2: The Variscan Cycle)*, *Deformation and Structure* (Vol. 10, pp. 307–348). https://doi.org/10.1007/978-3-030-10519-8

Simancas, J. F., Carbonell, R., González Lodeiro, F., Pérez Estaún, A., Juhlin, C., Ayarza, P., et al. (2003). The crustal structure of the transpressional Variscan orogen of SW Iberia. The IBERSEIS deep seismic profile. *Tectonics*, *22*(6), 1062. https://doi.org/10.1029/2002TC001479

Simancas, J. F., Martínez Poyatos, D., Expósito, I., Azor, A., & González Lodeiro, F. (2001). The structure of a major structure zone in SW Iberian Massif: The Ossa Morena/Central Iberian contact. *Tectonophysics*, *332*(1–2), 295–308. https://doi.org/10.1016/S0040-1951(00)00262-6

Terrinha, P. (1998). *Structural geology and tectonic evolution of the Algarve Basin, South Portugal* (PhD thesis) (pp. 1–430). Imperial College of London.

Tietze, K., & Ritter, O. (2013). Three-dimensional magnetotelluric inversion in practice—The electrical conductivity structure of the San Andreas Fault in Central California. *Geophysical Journal International*, *195*(1), 130–147. https://doi.org/10.1093/gji/ggt234

Tikhonov, A. N. (1950). On determining electrical characteristics of the deep layers of the Earth's crust. *Doklady Akademii Nauk*, *73*(2), 295–297.

Valle Aguado, B., Arenas, R., & Martínez Catalán, J. R. (1993). Evolución metamórfica hercínica en la región de la Serra de Arada (Norte de Portugal). *Comunicacoes do Instituto Geologico e Mineiro*, *79*, 41–61.

Veludo, I., Dias, N. A., Fonseca, P. E., Matias, L., Carrilho, F., Haberland, C., & Villaseñor, A. (2017). Crustal seismic structure beneath Portugal and southern Galicia (Western Iberia) and the role of Variscan inheritance. *Tectonophysics*, *717*, 645–664. https://doi.org/10.1016/j.tecto.2017.08.018

Vieira da Silva, N., Mateus, A., Monteiro Santos, F. A., Almeida, E. P., & Pous, J. (2007). 3-D electromagnetic imaging of a Palaeozoic plate-tectonic boundary segment in SW Iberian Variscides (S Alentejo, Portugal). *Tectonophysics*, *445*(1–2), 98–115. https://doi.org/10.1016/j.tecto.2007.06.006

Vozoff, K. (1991). The magnetotelluric method: Electromagnetic methods. In M. N. Nabighian (Ed.), *Applied Geophysics* (pp. 641–712).

Wannamaker, P. E. (2000). Comment on "The petrologic case for a dry lower crust" by Bruce W. D. Yardley and John W. Valley. *Journal of Geophysical Research*, *105*(B3), 6057–6064. https://doi.org/10.1029/1999jb900324

Wannamaker, P. E. (2002). Fluid generation and pathways beneath an active compressional orogen, the New Zealand Southern Alps, inferred from magnetotelluric data. *Journal of Geophysical Research*, *107*(B6), 2117. https://doi.org/10.1029/2001JB000186

Zhao, G., Unsworth, M. J., Zhan, Y., Wang, L., Chen, X., Jones, A. G., et al. (2012). Crustal structure and rheology of the Longmenshan and Wenchuan Mw 7.9 earthquake epicentral area from magnetotelluric data. *Geology*, *40*(12), 1139–1142. https://doi.org/10.1130/G33703.1